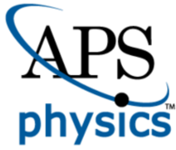

CHORUS

This is the accepted manuscript made available via CHORUS. The article has been published as:

Spontaneous Polarization in an Ultrathin Improper-Ferroelectric/Dielectric Bilayer in a Capacitor Structure at Cryogenic Temperatures

Yu Yun, Pratyush Buragohain, Arashdeep Singh Thind, Yuewei Yin, Xin Li, Xuanyuan Jiang, Rohan Mishra, Alexei Gruverman, and Xiaoshan Xu

Phys. Rev. Applied **18**, 034071 — Published 26 September 2022

DOI: 10.1103/PhysRevApplied.18.034071

Spontaneous polarization in ultrathin improper ferroelectric/dielectric bilayer in a capacitor structure at cryogenic temperature

Yu Yun*,[1] Pratyush Buragohain*,[1] Arashdeep Singh Thind,[2] Yuewei Yin,[1] Xin Li,[1]
Xuanyuan Jiang,[1] Rohan Mishra,[2,3] Alexei Gruverman,[1,4] and Xiaoshan Xu[1,4]

[1] *Department of Physics and Astronomy, University of Nebraska, Lincoln, NE 68588, USA*
[2] *Institute of Materials Science and Engineering, Washington University in St. Louis, St. Louis MO, USA*
[3] *Department of Mechanical Engineering and Materials Science, Washington University in St. Louis, St. Louis MO, USA*
[4] *Nebraska Center for Materials and Nanoscience, University of Nebraska, Lincoln, NE 68588, USA*

(Dated: September 8, 2022)

To determine the effect of depolarization and the critical thickness in the improper ferroelectric hexagonal ferrite thin films, we investigated the polarization switching of ferroelectric/dielectric bilayer in capacitor structures at 20 K. Experimentally, we show that the spontaneous polarization persists throughout the studied thickness range (3 to 80 unit cell), even with a thick (10 nm) dielectric layer, suggesting no practical thickness limit for applications. By fitting the effect of depolarization using the phenomenological theory, we show that the spontaneous polarization remain finite when the thickness of the ferroelectric layer approaches zero, providing a hint for the absence of critical thickness. We also find that the interfacial effects limit the multidomain formation and govern the polarization switching mechanisms.

I. INTRODUCTION

Ferroelectric (FE) materials exhibit switchable spontaneous polarizations, enabling applications in sensors, actuators, and non-volatile memory devices [1–3]. A well-known limiting factor of ferroelectrics that poses a scalability problem for applications is the critical thickness below which spontaneous polarization vanishes [4–7].

The electrostatic origin of the critical thickness is illustrated in Fig. 1(a), where the dielectric (DE) layer effectively represents the non-FE interfacial layer and the finite screening length of the electrodes. Due to the DE layer, under the short-circuit condition, the electric field generated by the polarization (P), called depolarization field, is not fully screened by the charges on the electrodes, resulting in a positive depolarization-field energy $U_{dep} \propto P^2$. For proper ferroelectrics, the spontaneous polarization is driven by the free-energy reduction also proportional to P^2; U_{dep} may then overcome the free-energy reduction and destabilize the spontaneous polarization [Fig. 1(b)] when the FE/DE thickness ratio is small enough, resulting in critical thickness.

The problem of critical thickness may be alleviated in improper ferroelectrics, where the spontaneous polarization is induced by the non-polar primary order that breaks the inversion symmetry. U_{dep} is expected to reduce but not necessarily quench the spontaneous polarization, as long as the primary order persists. Hence, it is imperative to study the polarization switching process in improper ferroelectrics, as a function of thickness to elucidate the effect of depolarization field, and down to the ultrathin limit to determine the existence of the critical thickness. However, this has been held back by the elusive DE layers and the entangled effects of the depolarization-field and the interface.

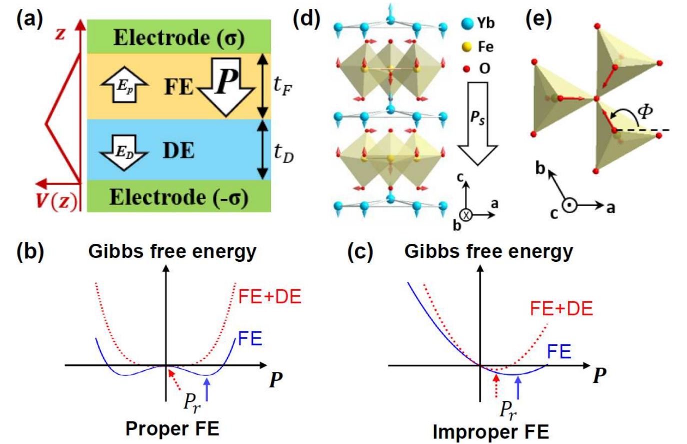

FIG. 1. (Color online) (a) Schematic diagram of the FE/DE bilayer structure at the short circuit condition. The electric field in both the FE and the DE layers are nonzero. Schematic of the Gibbs free energy for the single FE layer (solid) and the FE/DE bilayer capacitor (dashed) with proper FE (b) and improper FE (c) respectively. P_r is the spontaneous polarization. (d) The displacement pattern of the K_3 distortion in YFO. (e) K_3 phase angle Φ illustrated as the tilt direction of the FeO_5 bipyramids.

In this work, we focus on hexagonal ferrites, in which the linear coupling [Fig. 1(c)] between P and the non-polar primary K_3 structural distortion [Fig. 1(d) and (e)] [8–10] leads to the improper ferroelectricity. We adopt an FE/DE bilayer structure with a thick DE buffer layer ($t_D \geq 10$ nm) to allow quantitative control of the depolarization-field effect and to minimize the interfacial effects on the spontaneous polarization. The results demonstrate the persistent spontaneous polariza-

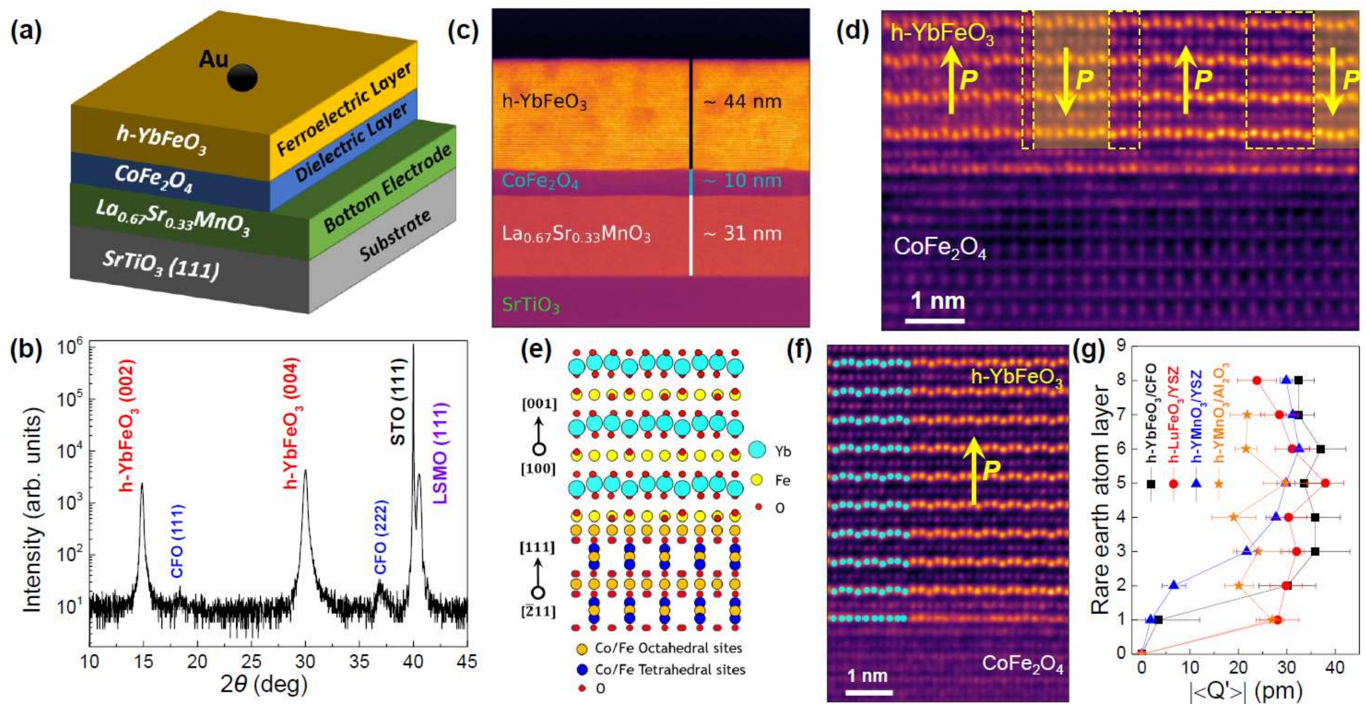

FIG. 2. (Color online) (a) Schematics of the YFO/CFO/LSMO/STO heterostructure. (b) Typical θ-2θ scan of XRD, with no obvious impurity peaks observed. (c) An HAADF-STEM image showing the heterostructure in (a). (d) HAADF-STEM image near the YFO/CFO interface showing a multidomain structure; the domain walls are marked by dashed-line boxes. (e) Atomic structure model of the YFO/CFO interface. (f) HAADF-STEM image near the YFO/CFO interface showing an up polarization in the YFO film, where the Yb atoms in the left part are highlighted. (g) Average displacement $| < Q' > |$ plotted again the distance from the interface, including data obtained from (f) and those obtained from the literature (see text).

tion even for the ultrathin (3 unit cell) ferroelectric layer with a thick (10 nm) DE layer, suggesting no practical thickness limit for applications. The interfacial effects play a key role in polarization switching mechanisms.

II. METHODS

The epitaxial heterostructure YFO/CFO/LSMO [Fig. 2(a)] has been grown using pulsed laser deposition (PLD) [11], where YFO (hexagonal $YbFeO_3$), CFO ($CoFe_2O_4$), and LSMO ($La_{0.67}Sr_{0.33}MnO_3$) are the FE layer, DE layer, and the bottom electrode respectively [see Supplementary Materials S1][12]. The CFO layer also serves as a buffer layer for epitaxial growth of YFO on LSMO to mitigate the large lattice mismatch [see Supplementary Materials S1]. The crystal structures were measured using x-ray diffraction (XRD). The ferroelectric hysteresis were measured using a Radiant Ferroelectric Tester with Au top electrodes of 200 - 400 μm diameter at low temperature using a closed-cycle Cryostat to minimize the sample leakage, and to avoid the possible semiconducting behavior due to the lattice mismatch [see Supplementary Materials S2]. The polarization switching dynamics were measured using a Keysight arbitrary waveform generator and a Tektronix oscilloscope. Scanning transmission electron microscopy (STEM) imaging was carried out using the aberration corrected Nion UltraSTEM200 microscope at the Oak Ridge National Laboratory.

III. RESULTS

A. Persistent K_3 distortion

As shown in Fig. 2(b), the typical θ-2θ scan is consistent with the structure in Fig. 2(a) with no indication of impurity. The crystal structures of the films near the YFO/CFO interface have been studied using STEM to determine whether the primary K_3 distortion persists down to the ultrathin limit, as discussed below.

A high-angle annular dark field (HAADF) image of the heterostructure is shown in Fig. 2(c), where the thicknesses of the layers is consistent with the fitting results of x-ray reflection (XRR) [Supplementary Materials S1][12]. Atomic resolution HAADF-STEM image for the YFO/CFO interface, viewed along the YFO [100] zone axis, is shown in Fig. 2(d); the corresponding crystal structural model is shown in Fig. 2(e). Since in the HAADF mode, the intensity is approximately proportional to the squared atomic number (Z^2) [13], the

brightest dots in Fig. 2(d) correspond to Yb atoms (Z = 70). The the buckling of the Yb layers, which is a key aspect of the K_3 distortion [Fig. 1 (d)], can be identified in Fig. 2(d); the vertical displacement of the Yb atoms $|<Q'>|$ is proportional to the K_3 magnitude Q [14, 15]. The displacement patterns, "two-up-one-down" or "one-up-two-down", correspond to polarization up and down respectively. The polarization direction can be mapped accordingly, revealing domains with opposing polarizations and the corresponding domain walls [Fig. 2(d)].

The buckling of the Yb layers is clearly reduced near the YFO/CFO interface, indicating the interfacial clamping effect, as reported previously in $YMnO_3$ (YMO) films grown on yttrium stabilized zirconia (YSZ) [14]. Based on the HAADF-STEM image of a YFO single domain in Fig. 2(f), we determined the Yb positions. Accordingly, the average vertical displacements $|<Q'>|$ of Yb atoms were extracted and plotted against the distance from the interface and compared with the results of interfaces with isomorphic materials (YMO and hexagonal $LuFeO_3$) from the literature [14, 16, 17], as shown in Fig. 2(g). The YMO/YSZ interface stands out as the reduction of $|<Q'>|$ is substantial up to 2 Y layers, which was attributed as part of the cause of the second-harmonic-response loss in the 2-unit-cell (4 layers) YMO films [14]. In contrast, only the very first Yb layer near the YFO/CFO interface show significantly reduced $|<Q'>|$, suggesting that the interfacial clamping effect is not expected to cause a critical thickness of ferroelectricity in YFO by suppressing $|<Q'>|$.

B. Spontaneous polarization at the ultrathin limit

Given that the K_3 distortion is likely to persists at the ultrathin limit, we studied the ferroelectric hysteresis of the FE/DE bilayer with different $\frac{t_F}{t_D}$ at 20 K and 500 Hz, using the PUND (positive-up-negative-down) method [18] [Supplementary Materials S2][12]. As shown in Fig. 3(a), the σ-V loops change dramatically with $\frac{t_F}{t_D}$, where σ is the area charge density on the electrodes and V is applied voltage. The remanence σ_r scales with $\frac{t_F}{t_D}$, indicating a dominant electrostatic effect, as shown in Fig. 3(b). For the FE/DE bilayer under the short-circuit condition ($V = 0$), the remanent charge (σ_r) and spontaneous polarization (P_r) follows

$$\sigma_r = \frac{P_r}{1 + \frac{\varepsilon_0 t_D}{\varepsilon_D t_F}}, \tag{1}$$

where ε_0 and ε_D are the permittivity of vacuum and the DE material, respectively [Supplementary Materials S4.1.1][12]. Under-screening is manifested as $\sigma_r \leq P_r$, which holds for both proper and improper ferroelectrics. Considering $\frac{\varepsilon_D}{\varepsilon_0} = 14$ for CFO [19], the variation of $\frac{\sigma_r}{P_r}$ estimated using Eq. (1) is much smaller than the observation in Fig. 3(b). Therefore, the change of σ_r must be

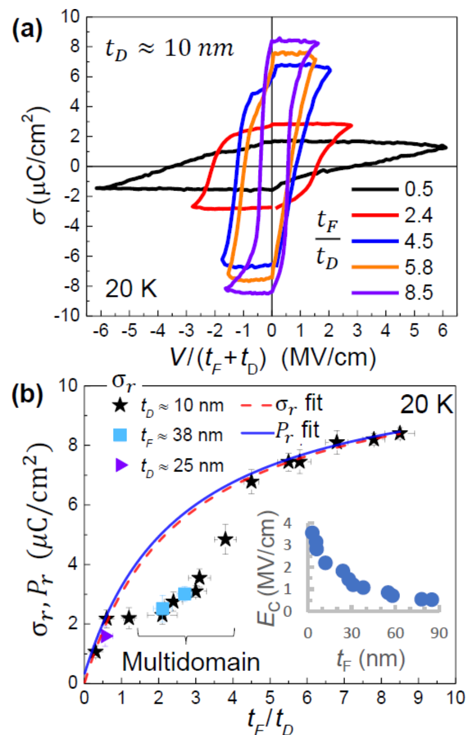

FIG. 3. (Color online) (a) Representative $\sigma - V$ loops with various $\frac{t_F}{t_D}$. (b) Remanence σ_r and P_r as a function of $\frac{t_F}{t_D}$. Inset: the t_F-dependence of coercivity E_C for t_D=10 nm. All measured at 20 K.

mainly due to the change of P_r as an effect of U_{dep}, as analyzed below.

As illustrated in Fig. 1 (a), under the short-circuit condition the magnitude of the voltage drop across the DE and FE layers are equal, which means $U_{dep} = \frac{1}{2}\frac{A^2}{C_{VF}+C_D}P^2$ as if the two layers are capacitors in parallel, where A is the area of the capacitor, $C_D \equiv \frac{A\varepsilon_D}{t_D}$ is the capacitance of the DE layer, and $C_{VF} \equiv \frac{A\varepsilon_0}{t_F}$ [Supplementary Materials S4.1.2][12]. For improper ferroelectric hexagonal ferrites, the lowest-order energy reduction by the spontaneous polarization is linear to P, as indicated by the Gibbs free energy of the FE/DE bilayer capacitor under the short-circuit condition according to the phenomenological theory: [Supplementary Materials S4.1.3.3][12, 20] $G = (g_0 - \alpha P + \frac{1}{2}\beta P^2)At_F + \frac{1}{2}\frac{A^2}{C_{VF}+C_D}P^2$, where g_0, α and β are coefficients that depend on the magnitude Q and phase Φ of the K_3 distortion. The linear term $-\alpha P$ is responsible for the spontaneous polarization. By minimizing G with respect to P, one finds

$$P_r = (1 + \frac{C_{VF}}{C_D})/(1 + \frac{C_F}{C_D})P_{rF} \tag{2}$$

where $P_{rF} \equiv \frac{\alpha}{\beta}$ is the spontaneous polarization without the DE layer and $C_F \equiv C_{VF}\frac{\beta\varepsilon_0+1}{\beta\varepsilon_0}$ is the effective capacitance of the FE layer. When $C_D \to 0$ ($\frac{t_F}{t_D} \to 0$, com-

pletely unscreened), P_r still has a finite value $\frac{C_{VF}}{C_F}P_{rF}$; this predicts that U_{dep} does not lead to a critical thickness for P_r.

As shown in Fig. 3(b), σ_r remains finite down to the ultrathin limit t_F= 3 nm (3 unit cell for YFO), with no obvious trend of dropping to zero at finite t_F which is also the case for P_r since $P_r \geq \sigma_r$ [Eq. (1)]. Specifically, Fig. 3(b) indicates P_r is greater than 10% of the saturation value at $\frac{t_F}{t_D}$=0.3, suggesting no practical thickness limit for device applications.

To quantitatively understand the effect of U_{dep}, we combine Eq. (1) and Eq. (2) and find the thickness dependence of σ_r as [Supplementary Materials S4.2.2.3][12]

$$\sigma_r = P_{rF}/(1+\frac{C_F}{C_D}) = P_{rF}/(1+\frac{C_F\varepsilon_0 t_D}{C_{VF}\varepsilon_D t_F}). \quad (3)$$

Eq. (3) agrees with the experiments in Fig. 3(b) in that σ_r increases with t_F/t_D.

For the small and large $\frac{t_F}{t_D}$ values, we fit the experimental data in Fig. 3(b) using Eq. (3); the result is plotted as the dashed line, with fitting parameters P_{rF}=10.9 ± 0.1 μC/cm^2 in agreement with the theoretical value of 9.6 μC/cm^2 for YFO [21], and $\frac{C_F}{C_{VF}}\frac{\varepsilon_0}{\varepsilon_D} = 2.60 \pm 0.07$ which means $\frac{C_F}{C_{VF}} \approx 36.4$ considering $\frac{\varepsilon_D}{\varepsilon_0} = 14$ for CFO [19], consistent with the direct measurements dielectric constants of the bilayers [Supplementary Materials Fig. S10][12]. The fitted P_r, calculated from the fitted σ_r using Eq. (1) is also plotted as the solid line in Fig. 3(b), which shows a finite value at $\frac{t_F}{t_D}$=0, providing a hint for the absence of critical thickness.

For the intermediate $\frac{t_F}{t_D}$ values, there is a rapid drop of σ_r. To explain the observation, we propose a scenario of multidomain formation consistent with the observation in Fig. 2(d) for a $\frac{t_F}{t_D}$= 4.4 film. Formation of multidomains can reduce U_{dep} at the cost of the domain-wall energy U_{dom}. For large t_F, U_{dep} is less than U_{dom} due to good screening, which is unfavorable for multidomains. For small t_F, if the interfacial contribution of U_{dom} is large, multidomains is also unlikely to form; this is consistent with the interfacial clamping observed in Fig. 2 and corroborated by the dramatic increase of coercivity E_C at smaller t_F in Fig. 3 (b) inset [22, 23]. For intermediate t_F, if the domain-wall stiffness is small, U_{dom} can be smaller than U_{dep} and drive the formation of multidomains. Earlier calculation found a small domain-wall stiffness in hexagonal manganites (isomorphic to YFO) due to the frustration-free nature of the domain walls [24]. Our analysis [Supplementary Materials S4.3][12] finds that the condition $\frac{t_F}{t_D}$ ≈4 (at which σ_r rapidly drops) agrees with the domain wall characteristics calculated for the YMO from first-principles [20] and the small grain size (≈10 nm) of the YFO films studied here; the latter is caused by the film/substrate structural mismatch and the resulting proliferation of anti-phase boundaries [Supplementary Materials S1][12].

C. Switching dynamics

In addition to the spontaneous polarization discussed above, we studied the YFO film of $\frac{t_F}{t_D} \approx 3.1$ at room temperature to elucidate the switching dynamics and the governing factors such as nucleation and domain wall motion processes, which are of great importance for understanding and applying improper ferroelectrics.[25]

As shown in Fig. 4(a), $\sigma - V$ loops were collected at different frequency using the PUND technique [Supplementary Materials S3][12] to remove the non-switching contributions. Coercive field E_C increases with the measurement frequency, as well-known in proper ferroelectrics. The switching dynamics in proper ferroelectrics has been broadly described by either the Kolmogorov-Avrami-Ishibashi (KAI) [26] model, in which the rate-limiting parameter is the domain wall velocity, or the nucleation limited switching (NLS) model [27], in which the rate-limiting parameter is the nucleation time for new domains. Bases on the KAI model and the NLS models, the frequency dependence of coercive fields has been derived as a power law $E_C \propto f^\beta$ [28] (Ishibashi-Orihara model) and a logarithmic dependence $\ln f = \ln f_0 + \frac{\alpha}{E_C^2}$ (Du-Chen model) respectively, where f is the measurement frequency and f_0 is the cutoff frequency [29] above which a nucleating domain cannot escape the potential well created by pinning centers. As shown in Fig. 4(b), E_C can be fit by both the two afore-mentioned models. The fitting with the power law leads to $\beta = 0.28$ for the YFO film, which is slightly larger than the values reported in the literature [28, 30–32] on other ferroelectric materials, suggesting possible differences in the switching mechanism from the pure domain wall motion. On the other hand, a cutoff frequency of ≈ 365 kHz was obtained which is within the range of proper ferroelectric thin films [33, 34]. Which model works better for the YFO films at room temperature can be answered by measuring the temperature dependent $E_C(f)$ relation [34] or using the square pulses [27] [Supplementary materials S3][12]; the latter is discussed below.

The switched polarization as a function of the pulse duration for different applied voltages using the above procedure is shown in Fig. 4(c), which has been fitted by the equation [27] $\Delta P(t) = 2P_S\int_{-\infty}^{\infty}[1 - e^{-(\frac{t}{t_0})^n}]F(\log t_0)d(\log t_0)$, where n=2 (for thin films) was used, and $F(\log t_0)$ is the distribution function of the characteristic switching time (t_0). For the KAI model [26], $F(\log t_0)$ is a delta function, while for the NLS model it is a Lorentzian function [35] given by $F(\log t_0) = \frac{A_0}{\pi}\frac{w}{(\log t_0 - \log t_1)^2 + w^2}$, where A_0 is a normalization constant, w is the half width at half-maximum, and $\log t_1$ is the central value of the distribution. The inset of Fig. 4(c) shows the corresponding distribution functions in the fitting of NLS model. The representative fitting results are displayed in Fig. 4(d), indicating that the

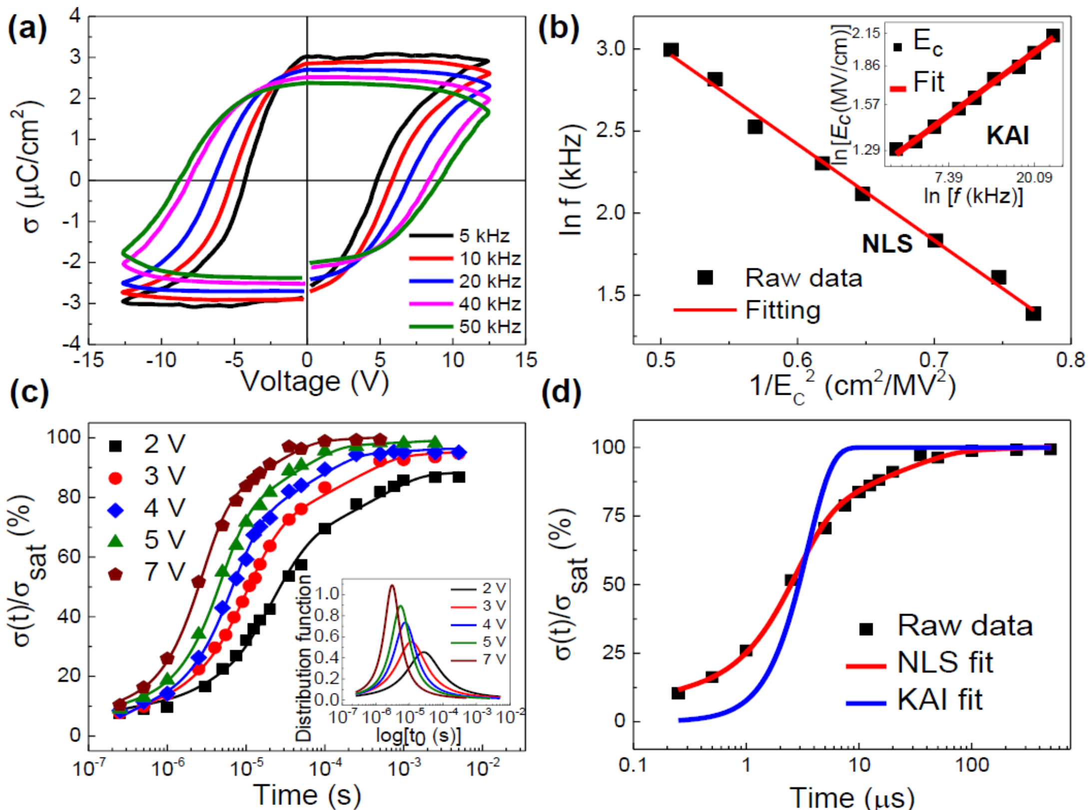

FIG. 4. (Color online) (a) Frequency-dependent $\sigma - V$ loops for the sample of $\frac{t_F}{t_D} \approx 3.1$ at room temperature. (b) Frequency-dependent coercive field fitted by the Du-Chen model. Inset: Fitting by the Ishibashi-Orihara model. (c) Switched σ as a function of time (t) under various external voltages. Inset: distribution function extracted from the NLS model. (d) Data from (c) at 7 V fitted by the KAI model and the NLS model.

switching process is better described by the NLS model with a distribution of switching time.

NLS model has been shown successful in describing polycrystalline ferroelectrics [27, 35–37], which can be considered as an ensemble of regions that switch independently. Although previous work indicates in $ErMnO_3$ (isomorphic to YFO) single crystals, domain wall motion dominates the switching process [32], the small grains and the surface pinning of the YFO films as revealed in the multidomain formation discussed above, is expected to cause a distribution of swithching time better described by the NLS model.

IV. Conclusion

In summary, we have experimentally shown that the spontaneous polarization of YFO persists throughout the thickness range studied (3 to 80 unit cell), suggesting no practical thickness limit in applications. The effect of depolarization field on the spontaneous polarization of YFO has been elucidated by quantitatively controlling the electrostatic effect and minimizing the interfacial effect using the FE/DE bilayer structures; the extrapolated spontaneous polarization remains finite at zero t_F/t_D. The film-substrate mismatch, which leads to the interfacial clamping and determines the film microstructure, causes significant interfacial domain pinning and the NLS switching dynamics. These results are a critical step toward device applications of improper ferroelectric hexagonal ferrites and manganites, especially for the design of miniaturized devices using ultrathin films.

ACKNOWLEDGMENT

This work was primarily supported by the National Science Foundation (NSF), Division of Materials Research (DMR) under Grant No. DMR-1454618. The research was performed in part in the Nebraska Nanoscale Facility: National Nanotechnology Coordinated Infrastructure and the Nebraska Center for Materials and Nanoscience, which are supported by the NSF under Grant No. ECCS-1542182, and the Nebraska Research Initiative. Work at Washington University was supported by NSF Grant No. DMR-1806147. STEM experiments were conducted at the Center for Nanophase Materials Sciences at Oak Ridge National Laboratory,

which is a Department of Energy (DOE) Office of Science User Facility, through a user project.

*Authors contribute equally.

[1] N. Setter, D. Damjanovic, L. Eng, G. Fox, S. Gevorgian, S. Hong, A. Kingon, H. Kohlstedt, N. Y. Park, G. B. Stephenson, I. Stolitchnov, A. K. Taganstev, D. V. Taylor, T. Yamada, S. Streiffer, Ferroelectric thin films: Review of materials, properties, and applications. J. Appl. Phys. 100, 051606 (2006).

[2] J. F. Scott, Ferroelectric Memories (Springer Press, Berlin/Heidelberg, Germany, 2000).

[3] J. F. Scott, Applications of Modern Ferroelectrics. Science 315, 954-959 (2007).

[4] J. E. Rault, W. Ren, S. Prosandeev, S. Lisenkov, D. Sando, S. Fusil, M. Bibes, A. Barthelemy, L. Bellaiche, N. Barrett, Thickness-Dependent Polarization of Strained BiFeO3 Films with Constant Tetragonality. Phys. Rev. Lett. 109, 267601 (2012).

[5] D. D. Fong, G. B. Stephenson, S. K. Streiffer, J. A. Eastman, O. Auciello, P. H. Fuoss, C. Thompson, Ferroelectricity in ultrathin perovskite films. Science 304, 1650-1653 (2004).

[6] J. Junquera, P. Ghosez, Critical thickness for ferroelectricity in perovskite ultrathin films. Nature 422, 506-509 (2003).

[7] Y. S. Kim, D. H. Kim, J. D. Kim, Y. J. Chang, T. W. Noh, J. H. Kong, K. Char, Y. D. Park, S. D. Bu, J. G. Yoon, J. S. Chung, Critical thickness of ultrathin ferroelectric BaTiO3 films. Appl. Phys. Lett. 86, 102907 (2005).

[8] M. Stengel, C. J. Fennie, P. Ghosez, Electrical properties of improper ferroelectrics from first principles. Phys. Rev. B 86, 094112 (2012).

[9] N. Sai, C. J. Fennie, A. A. Demkov, Absence of critical thickness in an ultrathin improper ferroelectric film. Phys. Rev. Lett. 102, 107601 (2009).

[10] C. J. Fennie, K. M. Rabe, Ferroelectric transition in YMnO3 from first principles. Phys. Rev. B 72, 100103(R) (2005).

[11] X. Zhang, Y. Yin, S. Yang, Z. Yang, X. Xu, Effect of interface on epitaxy and magnetism in h-RFeO3/Fe3O4/Al2O3 films (R = Lu, Yb). J. Phys. Condens. Matter 29, 164001 (2017).

[12] See Supplemental Material at http://link.aps.org/supplemental/XXX for more information on characterizations of structural and ferroelectric properties and the Landau theory analysis.

[13] S. J. Pennycook and D. E. Jesson, High-resolution Z-contrast imaging of crystals. Ultramicroscopy 37, 14-38 (1991).

[14] J. Nordlander, M. Campanini, M. D. Rossell, R. Erni, Q. N. Meier, A. Cano, N. A. Spaldin, M. Fiebig, M. Trassin, The ultrathin limit of improper ferroelectricity. Nat. Commun. 10, 5591 (2019).

[15] M. E. Holtz, K. Shayovalov, J. A. Mundy, C. S. Chang, Z. W. Yan, E. Bourret, D. A. Muller, D. Meier, A. Cano, Topological Defects in Hexagonal Manganites: Inner Structure and Emergent Electrostatics. Nano Lett. 17, 5883-5890 (2017).

[16] W. Wang, J. A. Mundy, C. M. Brooks, J. A. Moyer, M. E. Holtz, D. A. Muller, D. G. Schlom, W. Wu, Visualizing weak ferromagnetic domains in multiferroic hexagonal ferrite thin film. Phys. Rev. B 95, 134443 (2017).

[17] S. Cheng, C. Xu, S. Deng, M.-G. Han, S. Bao, J. Ma, C. Nan, W. Duan, L. Bellaiche, Y. Zhu, J. Zhu, Interface reconstruction with emerging charge ordering in hexagonal manganite. Sci. Adv. 4, eaar4298 (2018).

[18] M. Fukunaga, Y. Noda, New Technique for Measuring Ferroelectric and Antiferroelectric Hysteresis Loops. J. Phys. Soc. Jpn. 77, 064706 (2008).

[19] D. Gutierrez, M. Foerster, I. Fina, J. Fontcuberta, D. Fritsch, C. Ederer, Dielectric response of epitaxially strained CoFe2O4 spinel thin films. Phys. Rev. B 86, 125309 (2012).

[20] S. Artyukhin, K. T. Delaney, N. A. Spaldin, M. Mostovoy, Landau theory of topological defects in multiferroic hexagonal manganites. Nat. Mater. 13, 42-49 (2014).

[21] H. Das, A. L. Wysocki, Y. Geng, W. Wu, C. J. Fennie, Bulk magnetoelectricity in the hexagonal manganites and ferrites. Nat. Commun. 5, 2998 (2014)

[22] A. K. Tagantsev, Size effects in polarization switching in ferroelectric thin films. Integr. Ferroelectr. 16, 237-244 (1997).

[23] D. R. Callaby, Domain Wall Velocities and the Surface Layer in BaTiO3. J. Appl. Phys. 36, 2751-2760 (1965).

[24] Y. Kumagai, N. A. Spaldin, Structural domain walls in polar hexagonal manganites. Nat. Commun. 4, 1540 (2013).

[25] P. Barrozo, D. R. Smabraten, Y. L. Tang, B. Prasad, S. Saremi, R. Ozgur, V. Thakare, R. A. Steinhardt, M. E. Holtz, V. A. Stoica, L. W. Martin, D. G. Schlom, S. M. Selbach, R. Ramesh, Defect-Enhanced Polarization Switching in the Improper Ferroelectric LuFeO3. Adv. Mater. 32, 2000508 (2020).

[26] Y. T. Yoshihiro Ishibashi, Note on Ferroelectric Domain Switching. J. Phys. Soc. Jpn. 31, 506-510 (1971).

[27] A. K. Tagantsev, I. Stolichnov, N. Setter, J. S. Cross, M. Tsukada, Non-Kolmogorov-Avrami switching kinetics in ferroelectric thin films. Phys. Rev. B 66, 214109 (2002).

[28] Y. Ishibashi, H. Orihara, A theory of D-E hysteresis loop. Integr. Ferroelectr. 9, 57-61 (1995).

[29] X. Du, I.-W. Chen, Frequency Spectra of Fatigue of PZT and other Ferroelectric Thin Films. MRS Online Proc. Libr. 493, 311-316 (1997).

[30] J. F. Scott, Models for the frequency dependence of coercive field and the size dependence of remanent polarization in ferroelectric thin films. Integrated Ferroelectrics 12, 71-81 (2006).

[31] A. Ruff, A. Loidl, S. Krohns, Multiferroic Hysteresis Loop. Materials (Basel) 10, 1318 (2017).

[32] A. Ruff, Z. Y. Li, A. Loidl, J. Schaab, M. Fiebig, A. Cano, Z. W. Yan, E. Bourret, J. Glaum, D. Meier, S. Krohns, Frequency dependent polarisation switching in h-ErMnO3. Appl. Phys. Lett. 112, 182908 (2018).

[33] T. Tsurumi, S.-M. Num, Y.-B. Kil, S. Wada, High frequency measurements of P-E hysteresis curves of PZT thin films. Ferroelectrics 259, 43-48 (2001).

[34] D. J. Jung, M. Dawber, J. F. Scott, L. J. Sinnamon, J. M. Gregg, Switching Dynamics in Ferroelectric Thin Films: An Experimental Survey. Integr. Ferroelectr. 48, 59-68 (2010).

[35] J. Y. Jo, H. S. Han, J. G. Yoon, T. K. Song, S. H. Kim,

T. W. Noh, Domain switching kinetics in disordered ferroelectric thin films. Phys. Rev. Lett. 99, 267602 (2007).

[36] H. Mulaosmanovic, J. Ocker, S. Muller, U. Schroeder, J. Muller, P. Polakowski, S. Flachowsky, R. van Bentum, T. Mikolajick, S. Slesazeck, Switching Kinetics in Nanoscale Hafnium Oxide Based Ferroelectric Field-Effect Transistors. ACS Appl. Mater. Interfaces 9, 3792-3798 (2017).

[37] P. Buragohain, C. Richter, T. Schenk, H. Lu, T. Mikolajick, U. Schroeder, A. Gruverman, Nanoscopic studies of domain structure dynamics in ferroelectric La: HfO2 capacitors. Appl. Phys. Lett. 112, 222901 (2018).